Molecular dynamics simulations of flexible liquid crystal molecules using a Gay-Berne/Lennard-Jones model

Mark R. Wilson
Department of Chemistry, University of Durham, South Road, Durham, DH1 3LE, United Kingdom

(Received 14 July 1997; accepted 19 August 1997)

Molecular dynamics simulations are described for liquid crystal molecules composed of two Gay-Berne particles connected by an eight-site Lennard-Jones alkyl chain. Calculations have been carried out for 512 molecules in the *NVE* and *NPT* ensembles for simulation times of up to 6.4 ns. The system exhibits the sequence of phases: isotropic liquid, smectic-A, smectic-B, and the simulations demonstrate the spontaneous growth of a smectic-A liquid crystal over a period of approximately 6 ns on cooling from the isotropic liquid. Model molecules are seen to remain flexible and able to change conformation in the smectic-A phase. As temperature is reduced molecules become elongated as the number of *gauche* conformations drops, leading to a small increase in the spacing of smectic layers. The latter is seen through the temperature dependence of the Gay-Berne radial distribution function resolved parallel to the direction of orientational order. Results are presented which show an odd–even variation of orientational order parameters for bonds in the alkyl chain, and a change in effective torsional potentials as the system is cooled from isotropic liquid to a smectic-A phase. © *1997 American Institute of Physics.*
[S0021-9606(97)50444-2]

I. INTRODUCTION

Computer simulation has become a powerful tool for studying the structure and dynamical properties of liquid crystal phases. A range of models have been studied in recent years.[1] Hard nonspherical models have demonstrated the importance of excluded volume effects in promoting mesogenic behavior. Simulation of hard ellipsoids have shown the presence of nematic (N_+),[2,3] discotic nematic (N_-)[4] and biaxial nematic phases,[5,6] while studies of hard spherocylinders also show the presence of smectic phases.[7,8] Addition of attractive interactions to model molecules leads to a family of continuous nonspherical potentials including the Kihara potential,[9] the Gaussian overlap model[10] and the Gay-Berne potential.[11] The latter is related to a Lennard-Jones 12:6 pair potential in which both the well-depth ϵ and the range parameter σ depend on the relative orientation of the two particles. The Gay-Berne potential has proved to be particularly effective in modelling mesogenic systems and a large body of simulations which employ this model already exist.[12–16] A useful feature of the Gay-Berne potential is that it can easily be tuned to alter molecular shape and this has led to a variety of phases being successfully simulated. de Miguel *et al.*[17] have recently presented a systematic study of the effects of adjusting well-depth anisotropy, finding that the range of nematic stability is strongly influenced by this factor. Similar investigations have studied the effect on phase behavior of varying the molecular length/breadth ratio.[18] Some attempts have been made to parameterise the Gay-Berne potential to real liquid crystal molecules.[14] However, this task is far from easy and further work may be required to find the optimum way of relating Gay-Berne parameters to real systems. One other recent development is of particular note. Cleaver *et al.*[19] have written a generalized form of the Gay-Berne potential which is suitable for computing the interaction between dissimilar uniaxial or biaxial particles. This is an important development and may well facilitate a more realistic representation of rigid fragments of real liquid crystal molecules.

One feature of real liquid crystal molecules, which is (usually) neglected in the simulation of hard and soft nonspherical particles, is molecular flexibility. In many real liquid crystal molecules, flexible alkyl chains play a key role in determining mesophase stability. This has prompted a number of recent studies which have attempted to model liquid crystal molecules by the use of atomistic potentials.[20–31] These models are extremely expensive in terms of computer time. Such simulations require many more sites than are typically used for hard or soft nonspherical particles. Additional burdens also appear. In molecular dynamics (MD) work, the added demands of accurately modelling internal molecular structure limit acceptable MD time-steps to between 1 and 3 fs. These are rather shorter than the time-steps usually required to integrate rigid body motion for moderately anisotropic particles and this in turn leads to a requirement for longer simulation runs. In practice studies of realistic potentials have been limited to a few hundred picoseconds: long enough to equilibrate internal molecular structure, but too short to see the spontaneous formation of ordered phases from an isotropic fluid.

In the current study a hybrid Gay-Berne/Lennard-Jones model has been employed to study the phase behavior of a model liquid crystal dimer system composed of two mesogenic units linked via a flexible alkyl chain. There has been considerable interest in liquid crystal dimers, not the least because of the exceptionally large odd–even effects seen in the transition temperatures exhibited by homologues of varying chain length.[32–34] In the present study, the rigid mesogenic parts of liquid crystal dimer molecules are repre-

Downloaded 28 Sep 2005 to 129.234.4.10. Redistribution subject to AIP license or copyright, see http://jcp.aip.org/jcp/copyright.jsp

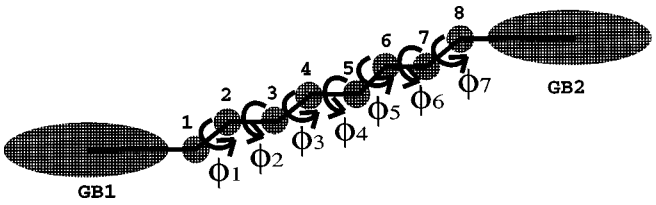

FIG. 1. The molecular structure for the model system studied. ϕ_i indicates dihedral angle i.

sented by Gay-Berne units, while the flexible chain is represented by an *united atom* Lennard-Jones chain. This type of hybrid model provides considerable savings in computer time over fully atomistic models. As a consequence of this, the current study is able to demonstrate the growth of a liquid crystalline phase from a completely isotropic system for the first time in an atom-based system.

The outline of this paper is as follows. Section II describes the simulation model employed, together with the molecular dynamics techniques used to study the phase behavior. The model described is similar to that employed by La Penna, Catalano and Veracini,[35] who have simulated a single Gay-Berne unit with an alkyl chain. However, there are a number of technical differences between the approach in Reference 35 and that adopted here. In Section III results are presented for simulations of 512 particles in both the *NVE* and *NPT* ensembles. Finally, in Section IV some conclusions are drawn.

II. COMPUTATIONAL MODEL

The model molecules used in this study have been made from a combination of anisotropic Gay-Berne and spherical Lennard-Jones sites (see Figure 1). The system is related to the liquid crystal dimer molecule α,ω-bis(4,4'-cyanobiphenyloxy)hexane, where the cyanobiphenyl moieties have been replaced by Gay-Berne sites. In the model system, bond lengths were fixed between the centres of adjacent sites and a potential of the form

$$E=\sum_{i=1}^{N_{\text{angles}}}\frac{k_i}{2}(\theta_i-\theta_i^o)^2+\sum_{i=1}^{N_{\text{dihedrals}}}\sum_{n=0}^{n=5}c_n(\cos\phi_i)^n+\sum_{i=1}^{N_{\text{LJ}}}\sum_{j>i}^{N_{\text{LJ}}}U_{ij}^{\text{LJ}}+\sum_{i=1}^{N_{\text{GB}}}\sum_{j>i}^{N_{\text{GB}}}U_{ij}^{\text{GB}}+\sum_{i=1}^{N_{\text{LJ}}}\sum_{j=1}^{N_{\text{GB}}}U_{ij}^{\text{LJ/GB}} \quad (1)$$

was used to model the intra- and intermolecular contributions to the interaction energy. In Equation (1), N_{angles}, $N_{\text{dihedrals}}$, N_{LJ} and N_{GB} are respectively the number of angles, number of dihedral angles, number of Lennard-Jones sites and number of Gay-Berne sites in the system; a harmonic potential is used to model bond angle deformation, where k_i is a bond angle force constant, θ_i and θ_i^o are actual and equilibrium bond angles; and a Ryckaert-Bellemans potential[36] is used to model changes in dihedral angles, where c_n is a coefficient in the expansion. U_{ij}^{LJ}, U_{ij}^{GB}, $U_{ij}^{\text{LJ/GB}}$ in Equation (1) represent nonbonded interactions energies for two particles i and j. The values of θ^o and k_i for the alkyl chain are taken from the work of Leggetter and Tildesley[37] who have simulated butane and decane chains. To reflect the C–O–C bond angle in the real liquid crystal dimer molecule, slightly larger angles are used for bond angles involving the Gay-Berne sites ($\theta^o=124^o58'$). In common with the Leggetter-Tildesley work, Ryckaert-Bellemans values[36] are used for the coefficients c_n. Because Gay-Berne sites are bonded via their center of masses, it is also necessary to include one additional harmonic angle term for each site bonded to a Gay-Berne particle. These terms involve the angle between the long axis of the Gay-Berne particle and the bond between the Gay-Berne site and the Lennard-Jones site to which it is attached. For these angles $\theta^o=180^o$, and the force constant is set at the value for a C–C–C bond angle. This term effectively prevents free rotation of Gay-Berne particles around their centres of mass.

The interaction energy U_{ij}^{LJ} for a separation r_{ij} is given by the standard Lennard-Jones 12:6 potential,

$$U_{ij}^{\text{LJ}}=4\epsilon_{ij}^{\text{LJ}}\left[\left(\frac{\sigma_{ij}^{\text{LJ}}}{r_{ij}}\right)^{12}-\left(\frac{\sigma_{ij}^{\text{LJ}}}{r_{ij}}\right)^{6}\right]. \quad (2)$$

For simplicity, and to substantially improve the speed of computation, only one type of Lennard-Jones atom has been used in this work. Values of $\epsilon_{ij}^{\text{LJ}}/k_b=72$ K and $\sigma_{ij}^{\text{LJ}}=3.923$ Å have been used, based on parameters for a CH_2 united-atom from Reference 37. U_{ij}^{GB} represents the orientational dependent interaction energy for two Gay-Berne particles:[10,11]

$$U_{ij}^{\text{GB}}=4\epsilon_0^{\text{GB}}[\epsilon^{\text{GB}}(\hat{\mathbf{u}}_i,\hat{\mathbf{u}}_j)]^{\nu}[\epsilon'^{\text{GB}}(\hat{\mathbf{u}}_i,\hat{\mathbf{u}}_j,\hat{\mathbf{r}}_{ij})]^{\mu}\times\left[\left(\frac{\sigma_0^{\text{GB}}}{r_{ij}-\sigma(\hat{\mathbf{u}}_i,\hat{\mathbf{u}}_j,\hat{\mathbf{r}}_{ij})+\sigma_0^{\text{GB}}}\right)^{12}-\left(\frac{\sigma_0^{\text{GB}}}{r_{ij}-\sigma(\hat{\mathbf{u}}_i,\hat{\mathbf{u}}_j,\hat{\mathbf{r}}_{ij})+\sigma_0^{\text{GB}}}\right)^{6}\right], \quad (3)$$

where $\hat{\mathbf{u}}_i$ and $\hat{\mathbf{u}}_j$ are unit vectors along the Gay-Berne molecular axes, σ is the orientation dependent distance of separation at which attractive and repulsive energies cancel and $\epsilon_0^{\text{GB}}[\epsilon^{\text{GB}}]^{\nu}[\epsilon'^{\text{GB}}]^{\mu}$ is the orientation dependent well depth. σ, $[\epsilon^{\text{GB}}]^{\nu}$ and $[\epsilon'^{\text{GB}}]^{\mu}$ are given by Equations (2)–(7) of reference 13. In the current work the form of the Gay-Berne potential studied by de Miguel *et al.*[12] has been used. In this form of the potential, $\mu=2$, $\nu=1$, the length to breadth ratio σ_{ee}/σ_{ss} is 3 and the ratio of well-depths for end-to-end and side-to-side particles $\epsilon_{ee}/\epsilon_{ss}$ is 1/5. In simulation studies of the Gay-Berne mesogen, the parameters σ_0^{GB}, ϵ_0^{GB} are normally set equal to unity and results are reported in terms of reduced units. In this work values of $\sigma_0^{\text{GB}}=\sigma_{ss}=4.721$ Å and $\epsilon_0^{\text{GB}}/k_b=\epsilon_{ss}/k_b=406.51$ K have been used. The value of σ_0^{GB} is taken from an average of the closest approach of two biphenyl rings in the three possible side-by-side configurations, the value of ϵ_0^{GB} is taken from References 35 and 38. In both of these papers, the form of the Lennard-Jones/Gay-Berne interaction between two particles $U_{ij}^{\text{LJ/GB}}$ is obtained by replacing the Gay-Berne potential by four atomic sites situated along the molecular long axis. However, a four-site Lennard-Jones molecule is rather different in shape to a Gay-Berne potential. Consequently, in this work a rather more

Downloaded 28 Sep 2005 to 129.234.4.10. Redistribution subject to AIP license or copyright, see http://jcp.aip.org/jcp/copyright.jsp

general form for $U_{ij}^{\mathrm{LJ/GB}}$ has been used based on the original work of Berne and Pechukas[10] who give the shape parameter for a rod-sphere interaction and the more recent work of Cleaver *et al.*,[19] who derive a generalized potential for two un-like Gay-Berne particles. Accordingly,

$$U_{ij}^{\mathrm{LJ/GB}} = 4\epsilon_0^{\mathrm{LJ/GB}}[\epsilon^{\mathrm{LJ/GB}}]^{\mu}(\hat{\mathbf{u}}_j, \hat{\mathbf{r}}_{ij}) \times \left[\left(\frac{\sigma_0^{\mathrm{LJ/GB}}}{r_{ij} - \sigma^{\mathrm{LJ/GB}}(\hat{\mathbf{u}}_j, \hat{\mathbf{r}}_{ij}) + \sigma_0{}^{\mathrm{LJ/GB}}} \right)^{12} - \left(\frac{\sigma_0^{\mathrm{LJ/GB}}}{r_{ij} - \sigma^{\mathrm{LJ/GB}}(\hat{\mathbf{u}}_j, \hat{\mathbf{r}}_{ij}) + \sigma_0{}^{\mathrm{LJ/GB}}} \right)^{6} \right], \tag{4}$$

where $\sigma^{\mathrm{LJ/GB}}$ and $\epsilon^{\mathrm{LJ/GB}}$ are given respectively by Equations (20) and (37) of Reference 19. In this work, values of $\sigma_0^{\mathrm{LJ/GB}} = 4.117$Å and $\epsilon_0^{\mathrm{LJ/GB}}/k_b = \sqrt{(}\epsilon^{\mathrm{LJ}}\epsilon_0^{\mathrm{GB}}/k_b = 171.08$ K were used. Spherical nonbonded cutoffs of 9.8075 Å, 18.884 Å, and 16.4679 Å, were employed for each of the pairwise-interactions U_{ij}^{LJ}, U_{ij}^{GB}, $U_{ij}^{\mathrm{LJ/GB}}$. For interactions involving Gay-Berne particles the cutoffs have been set at $4\times\sigma_0^{\mathrm{GB}}$ and $4\times\sigma_0^{\mathrm{LJ/GB}}$ respectively in common with standard simulations of Gay-Berne systems and the potential has been shifted to allow the interaction energy to go smoothly to zero at the cutoff.[16] To speed computation a separate Verlet neighbor list has been employed for each of the three sets of interactions. In calculating the intramolecular contributions to U_{ij}^{LJ}, $U_{ij}^{\mathrm{LJ/GB}}$, U_{ij}^{GB} in Equation (1) all interactions between 1–2, 1–3 and 1–4 bonded sites have been excluded.

The equations of motions were integrated using a form of the leap-frog algorithm suitable for anisotropic systems.[39,40] Bond lengths were fixed to a tolerance of $1.0 \times 10^{-}6$ Å using the SHAKE procedure of Ryckaert.[41] Initial calculations were carried out in the *NVE* ensemble using a time-step of 2 fs. Later calculations employed the *NPT* ensemble using the Anderson thermostat[42,43] and implementing a Monte Carlo procedure to alter the volume of the system V. Following Eppenga and Frenkel,[44] changes were made in $\ln V$. A random number δ was chosen uniformly from the range $(-\delta_{\max}, \delta_{\max})$, giving a new volume

$$V_{\mathrm{new}} = V_{\mathrm{old}} \exp(\delta), \tag{5}$$

with $\delta_{\max}$ chosen to allow acceptance ratios in the range 35–50%. For isotropic scaling of the system the length scaling factor is given by $\exp(\delta/3)$. For anisotropic scaling, a box dimension L_x, L_y, L_z was chosen at random with the box length scaling factor given by $\exp(\delta)$. Both isotropic and anisotropic scaling methods were tried for different state points. At the highest densities, anisotropic scaling was used exclusively, allowing the box shape to vary. This avoids the possibility of translationally ordered phases forming with layers which are incommensurate with the box dimensions. The scaling procedure adopted involved multiplying molecular centres of mass by the appropriate scaling factor and moving the whole molecule accordingly while keeping internal molecular configuration fixed.[45] Trial moves were accepted with a probability equal to $\min(1, \exp(-\beta\Delta H))$, where

$$\beta\Delta H = \beta\Delta E + \beta P\Delta V - (N_m + 1)\delta. \tag{6}$$

Here, N_m is the number of molecules, $\beta = 1/kT$, ΔE is the potential energy change in going from the old state to the new one.

III. RESULTS AND DISCUSSION

A. Phase behavior

Initial simulations were started from a low density array of molecules in an *all-trans* conformation aligned parallel to the z axis of the simulation box. Molecules were arranged with a random center of mass vector and atomic velocities taken from a Maxwell-Boltzmann distribution. This low density configuration was rapidly compressed to a density of 715.72 kgm^{-3} to provide a pseudo-nematic starting configuration. This density is somewhat lower than that expected for the real system, but reflects the observation by La Penna, Catalano and Veracini[35] that the effective volume of a Gay-Berne particle is rather larger than that of a real mesogen with similar mass and length/breadth ratio. This configuration was melted at 500 K, then equilibrated at 400 K to produce an isotropic starting configuration. The isotropic and pseudo-nematic starting configurations were used in a parallel series of simulations to map out the preliminary phase diagram at fixed volume at a range of energies in the *NVE* ensemble. During the simulations, orientational and translational ordering of the Gay-Berne sites was monitored; the former through the calculation of the orientational order parameter $S_2 = \langle P_2(\cos(\theta)) \rangle$ and the latter through the radial distribution function

$$g(r) = \frac{V}{[N_{\mathrm{GB}}]^2} \left\langle \sum_{i}^{N_{\mathrm{GB}}} \sum_{j \neq i}^{N_{\mathrm{GB}}} \delta(\mathbf{r} - \mathbf{r}_{ij}) \right\rangle, \tag{7}$$

where $\mathbf{r}_{ij}$ is the vector between the centres of mass of Gay-Berne particles i and j. In this work, S_2 was associated with the largest eigenvalue λ_+ obtained through the diagonalization of the ordering tensor,

$$Q_{\alpha\beta} = \frac{1}{N_{\mathrm{GB}}} \sum_{j=1}^{N_{\mathrm{GB}}} \frac{3}{2} u_{j\alpha} u_{j\beta} - \frac{1}{2}\delta_{\alpha\beta}, \quad \alpha, \beta = x, y, z. \tag{8}$$

The eigenvector associated with λ_+ provides the director $\mathbf{n}$ describing the average direction of alignment for Gay-Berne particles. The direction of $\mathbf{n}$ was found to vary slowly during the course of the simulations. Consequently, a new director was computed for each set of coordinate data used in the compilation of $g(r)$. This allowed $g(r)$ to be resolved into two components $g_{\parallel}(r)$ and $g_{\perp}(r)$ which were used to respectively monitor translational order parallel and perpendicular to the director.

Extensive runs at $\langle T \rangle \approx 390$ K and $\langle T \rangle \approx 349$ K indicated a transition to an orientationally ordered phase between these temperatures. At $\langle T \rangle \approx 390$ K, the pseudo-nematic configuration required in excess of 3 ns simulation time to decay to an isotropic liquid. At $\langle T \rangle \approx 349$ K, an orientationally ordered phase grew spontaneously from an isotropic liquid over a period of 6 ns. Viewing of snapshots from equilibrated con-

Downloaded 28 Sep 2005 to 129.234.4.10. Redistribution subject to AIP license or copyright, see http://jcp.aip.org/jcp/copyright.jsp

TABLE I. Summary of simulation data in *NVE* ensemble. Quoted values of order parameters are for Gay-Berne units.

$\langle T \rangle$ /K	Phase	Equilibration time / ps	Production time / ps	E_{tot} /10^{-20} J	$\langle S_2 \rangle$
455.5	isotropic	1550	400	4540	0.04
389.2	isotropic	400	400	3002	0.14
378.3	smectic-A	1850	800	1678	0.66
326.4	smectic-A	850	1000	290.9	0.69
292.1	smectic-B	800	400	−1609	0.83
264.2	smectic-B/ solid	1000	1400	−2250	0.82

TABLE II. Summary of simulation data in *NPT* ensemble. Quoted values of order parameters are for Gay-Berne units.

$\langle T \rangle$ /K	Phase	Equilibration time / ps	Production time / ps	$\langle V \rangle$ /10^5 Å^3	$\langle S_2 \rangle$
400	isotropic	3400	2000	14.0 ± 0.6	0.01
370	isotropic	3000	2000	8.59 ± 0.3	0.05
330	isotropic	1000	1000	6.95 ± 0.1	0.10
310	smectic-A	5400	1000	4.76 ± 0.1	0.71
300	smectic-A	1200	800	4.90 ± 0.1	0.75
275	smectic-B	800	600	4.55 ± 0.1	0.83
235	smectic-B	1200	800	4.33 ± 0.1	0.86
175	smectic-B/ solid	400	400	4.19 ± 0.1	0.87

figurations at $\langle T \rangle \approx 349$ K, combined with extensive analysis of the degree of translational ordering (discussed in detail below), indicated that the orientationally ordered phase was a smectic-A phase. These simulations are considerably longer than any previous runs for atomistic mesogens, and represent (to the authors' best knowledge) the first atomistic simulations to conclusively demonstrate the growth of a smectic phase from an isotropic liquid. The full series of equilibrated state points from simulations in the *NVE* ensemble are summarized in Table I.

To check if the presence of a smectic phase was influenced by the fixed periodic boundary conditions in the *NVE* ensemble, a second series of simulations was carried out in the *NPT* ensemble. A stable isotropic phase was exhibited at 330 K, but reducing the temperature to 310 K immediately led to fluctuations in the value of S_2 and the growth of a stable orientationally ordered phase over a period of approximately 6 ns as shown in Figure 2. As with the *NVE* work, visualization indicated the presence of smectic layers. Details of *NPT* state-points studied are included in Table II. The ordering of molecules into layers is most clearly seen through the behavior of the functions $g(r)$, $g_\parallel(r)$, $g_\perp(r)$ calculated for Gay-Berne sites (Figure 3). In the pretransitional region of the isotropic phase a small first peak in $g(r)$ indicates only weak correlation between neighbouring sites. At lower temperatures $g(r)$ takes on the appearance of a well-ordered system with a substantial first solvation peak which grows in magnitude as temperature is reduced and develops additional peaks at larger values of r. The full picture is provided by the parallel and perpendicular components $g_\parallel(r)$, $g_\perp(r)$. $g_\parallel(r)$ indicates the presence of smectic layers with a layer spacing of approximately 32.5 Å. The peak at r/Å=13 corresponds to two adjacent layers of Gay-Berne units (in separate smectic layers) and the peak at r/Å=20.2 picks up the intramolecular correlation between 2 Gay-Berne sites in the same molecule. A small but detectable shift of the r/Å=20.2 and r/Å=32.5 peaks to larger r (+0.5 Å) occurs as temperature falls. This can be attributed to a molecular

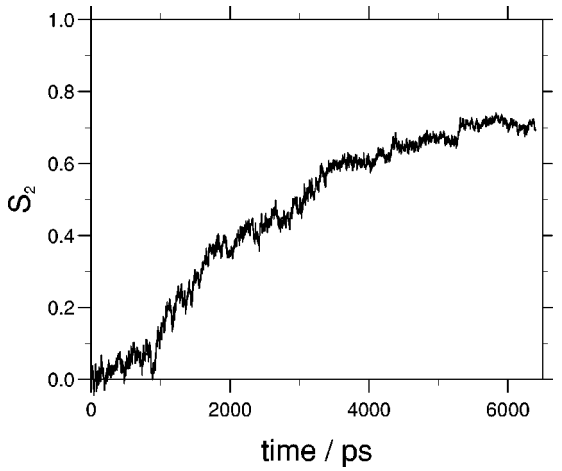

FIG. 2. Spontaneous growth of an orientationally order phase at 310 K in the *NPT* ensemble.

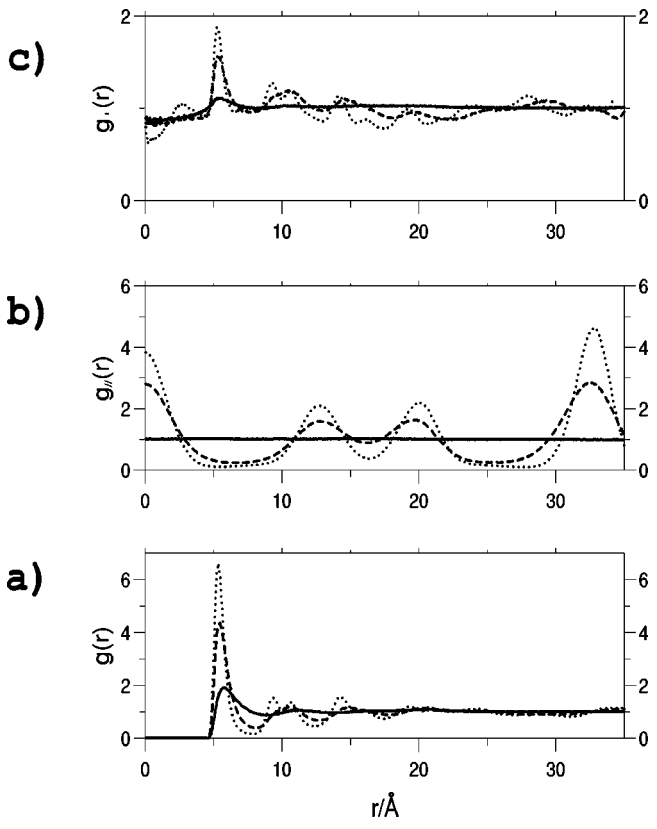

FIG. 3. Radial distribution functions for Gay-Berne sites in the *NPT* ensemble. (a) g(r); (b) $g_\parallel$; (c) $g_\perp$: bold line—330 K (isotropic phase, pretransitional region), dashed line—300 K (smectic-A phase), dotted line—235 K (smectic-B phase).

Downloaded 28 Sep 2005 to 129.234.4.10. Redistribution subject to AIP license or copyright, see http://jcp.aip.org/jcp/copyright.jsp

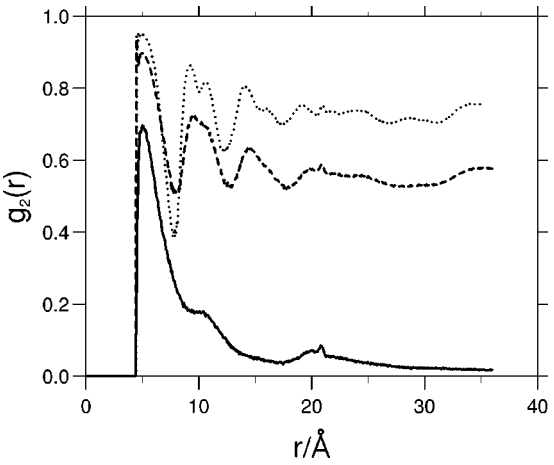

FIG. 4. The temperature dependence of the pairwise orientational correlation function g_2(r) for Gay-Berne centres in the NPT ensemble: lines denoted as in Figure 3.

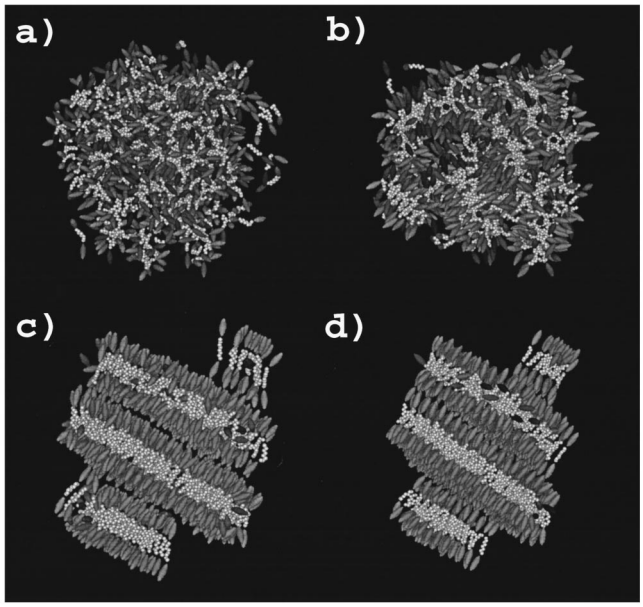

FIG. 5. Snapshots from simulations in the NPT ensemble. (a) Isotropic phase at 370 K; (b) isotropic phase at 330 K (showing pretransitional ordering); (c) smectic-A phase at 300 K; (d) smectic-B phase at 235 K. Gay-Berne sites are denoted by grey ellipsoids; Lennard-Jones sites are denoted by white spheres.

elongation which occurs as the temperature is reduced. The perpendicular component, $g_\perp(r)$, can be used to monitor intra-layer order. In comparing the system at 330 K and 235 K, the increase in size of the first solvation peak and the splitting of the second peak at $r/\text{Å}=10$ into two are indicative of the change from smectic-A (fluid) order to smectic-B (hexagonal) packing of Gay-Berne units within the layers. The change in order within the layers is also clearly visible in the behavior of the pairwise orientational correlation function $g_2(r)$ calculated for Gay-Berne sites (Figure 4)

$$g_2(r)=\langle P_2(\cos\ \theta_{ij}(r))\rangle, \tag{9}$$

where θ_{ij} is the angle between sites i and j and the ensemble average includes all pairs of Gay-Berne particles. In the isotropic phase at 330 K this function decays to zero at large r, but in an orientationally ordered phase tends to a value of $\langle S_2\rangle^2$ at large r. In Figure 4, the change in order in going from the smectic-A phase to the smectic-B phase is clearly visible in the form of the $g_2(r)$ at the temperatures 300 K and 235 K. In particular, the deepening of the troughs at $r/\text{Å}\approx 7.7$ and $r/\text{Å}\approx 12.5$ and the splitting of the peak at $r/\text{Å}\approx 10$ indicate the onset of hexagonal ordering within the layer. In all the curves in Figure 4, intramolecular correlations between two Gay-Berne units within the same molecule show up as small peaks in $g_2(r)$, with the most popular conformation (*all-trans*) showing as a small blip at $r/\text{Å}\approx 21$.

Visualization of snapshots from the simulations confirms the picture of molecular order provided by $g(r)$, and $g_2(r)$. In Figure 5 molecular configurations are plotted for four temperatures in the NPT ensemble. At high temperatures in the liquid phase there is no evidence for strong correlation between Gay-Berne units (Figure 5(a)). However, close to the liquid crystal phase transition (Figure 5(b)), in the isotropic pretransitional region, there is clear evidence for local smectic ordering and the first suggestions that the system would prefer to segregate into Gay-Berne rich and Lennard-Jones rich domains. Smectic-A layers are clearly visible at 330 K (Figure 5(c)), and in going from the smectic-A phase to the smectic-B phase (Figure 5(d)) layers become less fluid and better defined. A useful visual representation of the order of Gay-Berne centres is provided by joining the centres of all Gay-Berne units which lie within a 6 Å radius of each other. In Figure 6 this is displayed for snapshot configurations at 330 K, 235 K and the lowest temperature studied 175 K. The change in hexagonal order in going from the smectic-A (Figure 6(a),(b)) to smectic-B phase (Figure 6(c),(d)) is clearly seen. At 175 K, monitoring of the diffusion coefficient for Gay-Berne and Lennard-Jones centres suggests that the system is frozen. At this temperature there is some evidence for correlation between Gay-Berne centres for well-ordered domains in Figure 6(f), suggesting that it may be possible to distinquish between a higher temperature smectic-B phase and a low temperature crystal-B phase. The preferred packing is for the Gay-Berne unit in the layer above to lie in the center of an edge made by the triangular lattice of Gay-Berne units below, rather than in the center of the triangle. However, some defects remain in the hexagonal layer packing at 175 K (Figure 6(e)) and much larger system sizes would be required to study this effect in detail.

Examination of results for S_2, $g(r)$, $g_\parallel(r)$ and $g_\perp(r)$ for all state-points studied, together with visualization of snapshots, allows a final unambiguous assignment of phase behavior. These assignments have been included in Tables I (NVE ensemble) and II (NPT ensemble). It is interesting to compare these results with the work of de Miguel *et al.*[12] who have examined the phase diagram for Gay-Berne particles without alkyl tails. At zero pressure the Gay-Berne fluid exhibits a smectic-B phase but no smectic-A phase or nematic phase is seen (although a nematic phase is seen at higher pressures). However, if the length/breadth ratio of the Gay-Berne particle is increased[18] the effect on phase behav-

Downloaded 28 Sep 2005 to 129.234.4.10. Redistribution subject to AIP license or copyright, see http://jcp.aip.org/jcp/copyright.jsp

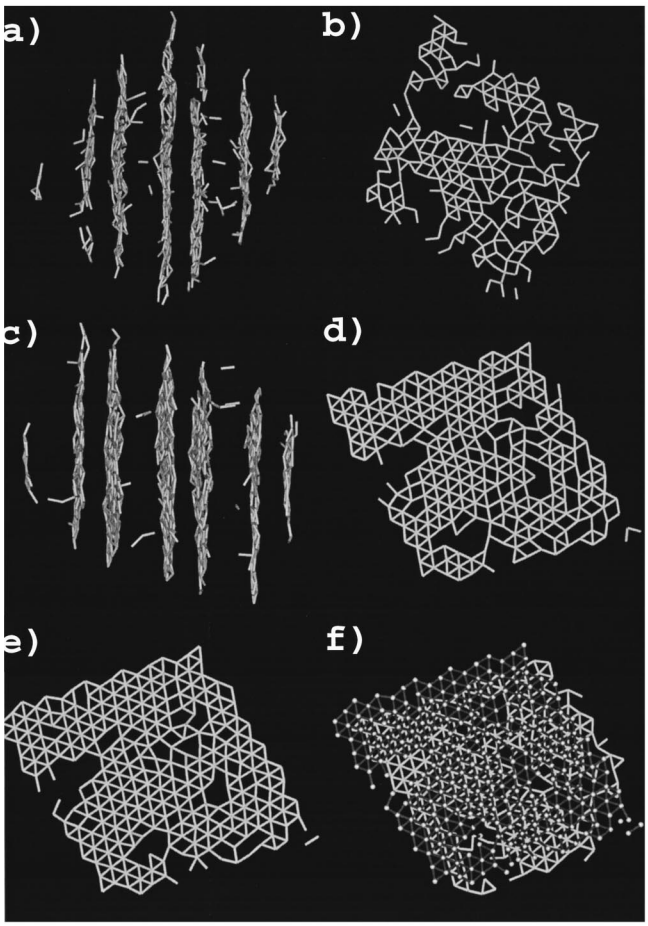

FIG. 6. Snapshots from simulations in the *NPT* ensemble showing *bonds* joining Gay-Berne centres of separation <6 Å: (a) smectic-A phase at 300 K (viewed perpendicular to the director); (b) smectic-A phase at 300 K (single layer viewed down the director); (c) smectic-B phase at 235 K (viewed perpendicular to the director); (d) smectic-B phase at 235 K (single layer viewed down the director); (e) smectic-B phase at 175 K (viewed down the director); (f) smectic-B phase at 175 K (adjacent layers viewed down the director).

ior is to increase the stability of the nematic phase and introduce a smectic-A phase. In the current work the effect of a flexible alkyl chain spacer between two Gay-Berne particles is to promote smectic-A phases by destabilizing the smectic-B phase. The strong Gay-Berne/Gay-Berne interactions however encourage segregation into Gay-Berne rich and Lennard-Jones rich domains and so no nematic phase is observed in this study.

B. Molecular structure

Replacing the vector u_j in Equation (8) by bond vectors allows individual order parameters to be calculated for each bond in the molecule (Table III). The values of bond order parameters exhibit a classic odd–even effect which increases in magnitude as the temperature is reduced. For an *all-trans* conformation successive bonds alternately lie parallel and at an angle to the molecular long axis. The bonds lying along the molecular long axis have high order parameters. This effect is well-known and for dimer molecules of this type

TABLE III. Order parameters for bonds in the alkyl chain.

$\langle S_2 \rangle$	300 K	275 K	235 K
Gay-Berne	0.75	0.83	0.86
bond 1–2	0.06	0.08	0.07
bond 2–3	0.61	0.72	0.77
bond 3–4	0.07	0.09	0.09
bond 4–5	0.61	0.71	0.76
bond 5–6	0.08	0.10	0.11
bond 6–7	0.62	0.71	0.75
bond 7–8	0.08	0.09	0.09

leads to a strong odd–even effect in the transition temperatures of a homologous series of molecules with varying chain lengths.[32,34] The increase in bond order parameters as temperature is reduced points to conformational changes within the molecule (discussed below). In all cases bond order parameters are smaller than the order parameters for the Gay-Berne units, indicating the importance of the latter in determining the overall structure of the bulk liquid crystal.

Comparison of a series of molecular configurations at 2 ps intervals confirms that internal molecular structure changes with temperature. At 300 K (smectic-A phase) a mean figure of 73 conformational changes occur between snapshots, and there is a strong preference for changes to the even dihedrals (ϕ_2, ϕ_4, ϕ_6) with a mean rate of change of $4.4\times$ the rate of change for the odd dihedrals (ϕ_1, ϕ_3, ϕ_5, ϕ_7). The high barrier to direct interconversion of *gauche* conformations in the Ryckaert-Bellemans potential means that no *gauche–gauche* transitions are detected and at conformational equilibrium an equal number of transitions to and from *trans* conformations are detected. As temperature is reduced further the mean rate of conversion of conformers drops considerably. At 275 K (assigned smectic-B above) the rate of transition drops to a mean of 15 conformational changes between 2 ps snapshots, and at the lowest temperature considered (175 K) the rate drops to a rate of 2 changes per snapshot. For the latter system, it appears that the conformational changes only occur in the region of defects in the solid structure. Even at the lowest temperature studied there are approximately equal numbers of transitions to and away from *trans* conformations, and so there is no evidence for a slow annealing to a completely *all-trans* structure.

The change in molecular structure with temperature is reflected through dihedral angle distributions $S(\phi)$. Figure 7 plots $S(\phi)$ for $\phi_1-\phi_4$ in the pretransitional region at 330 K and the smectic-A phase at 300 K ($S(\phi)$ plots for $\phi_5-\phi_7$ are respectively identical to those for $\phi_1-\phi_3$). A clear odd–even effect is visible for $S(\phi_i)$ with the odd dihedrals having substantially more molecules with *trans* conformations in the smectic-A phase. This odd–even effect is also visible in the pretransitional region, but to a much smaller extent. Integrating the dihedral angle distributions provides *trans*/*gauche* populations. In Table IV these are given for three temperatures which span the phase diagram. *Trans*/*gauche* populations are strongly influenced by the increase in molecular orientational order. As temperature is reduced, and molecules become increasingly ordered, the difference in *trans*

Downloaded 28 Sep 2005 to 129.234.4.10. Redistribution subject to AIP license or copyright, see http://jcp.aip.org/jcp/copyright.jsp

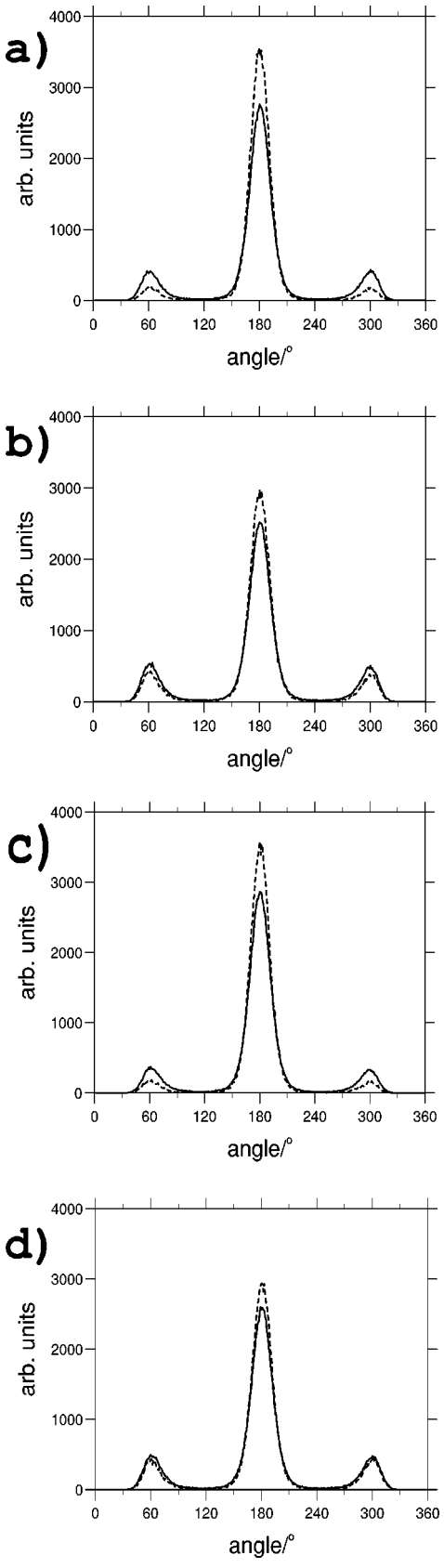

FIG. 7. Dihedral angle distribution in the NPT ensemble. (a) ϕ_1; (b) ϕ_2; (c) ϕ_3; (d) ϕ_4: bold line—330 K (isotropic phase), dashed line—300 K (smectic-A phase).

TABLE IV. *Trans-gauche* populations for selected state-points in the NPT ensemble.

$\langle T \rangle$/K	Phase	Dihedral	g_-/%	t/%	g_+/%
330	isotropic	ϕ_1	11.6	78.0	10.4
		ϕ_2	14.0	73.3	12.8
		ϕ_3	9.5	81.8	8.7
		ϕ_4	12.8	74.8	12.4
		ϕ_5	9.4	81.7	8.9
		ϕ_6	13.3	74.0	12.9
		ϕ_7	10.8	78.4	10.8
300	smectic-A	ϕ_1	4.7	90.5	4.8
		ϕ_2	10.4	80.3	9.4
		ϕ_3	4.3	92.0	3.7
		ϕ_4	10.0	79.6	10.4
		ϕ_5	3.3	92.5	4.2
		ϕ_6	9.1	81.4	9.6
		ϕ_7	4.5	91.5	4.1
235	smectic-B	ϕ_1	2.8	96.0	1.2
		ϕ_2	6.0	87.9	6.1
		ϕ_3	0.8	97.2	2.0
		ϕ_4	6.8	86.6	6.6
		ϕ_5	1.7	96.1	2.1
		ϕ_6	4.6	89.7	5.7
		ϕ_7	3.3	94.2	2.5

populations between odd and even dihedrals increases from a mean of approximately 6 percentage points in the pretransitional region to approximately 11% at 300 K in the smectic-A phase. However, in the smectic-B phase the molecules increasingly adopt an *all-trans* conformation. This leads to a drop in the *trans*/*gauche* odd–even effect in the smectic-B phase as the number of *trans* conformations starts to saturate for $\phi_1, \phi_3, \phi_5, \phi_7$.

Following Wilson and Allen,[21] the dihedral angle distribution can be written in the following form

$$S(\phi) = C \exp\left[-\frac{V(\phi)}{k_B T} \right], \tag{10}$$

where C is a normalization factor and $V(\phi)$ is an effective torsional potential or conformational free energy. $V(\phi)$ is composed of contributions from both intramolecular interactions V_{int} (mainly the Ryckaert-Bellemans potential and 1–5 nonbonded interactions), and an intermolecular part V_{ext} which depends strongly on molecular environment. Extracting $V(\phi)$ from Equation (10) in different phases provides a convenient *temperature independent* probe of the influence of molecular environment on molecular structure. Figure 8 shows a comparison between the effective torsional potentials at 300 K and 330 K and the Ryckaert-Bellemans potential. The potential in the pretransitional (330 K) region and that at a higher temperature (370 K) in the isotropic phase are almost identical. This suggests that the differences between the Ryckaert-Bellemans curve and $V(\phi)$ in the liquid phase can be attributed to intramolecular interactions, and a intermolecular contribution to $V(\phi)$ which is largely temperature independent. In contrast the differences between the potential at 300 K and 330 K can be directly attributed to the intermolecular component of $V(\phi)$ which changes in going from the isotropic to the smectic-A phase. In Figure 8 this

Downloaded 28 Sep 2005 to 129.234.4.10. Redistribution subject to AIP license or copyright, see http://jcp.aip.org/jcp/copyright.jsp

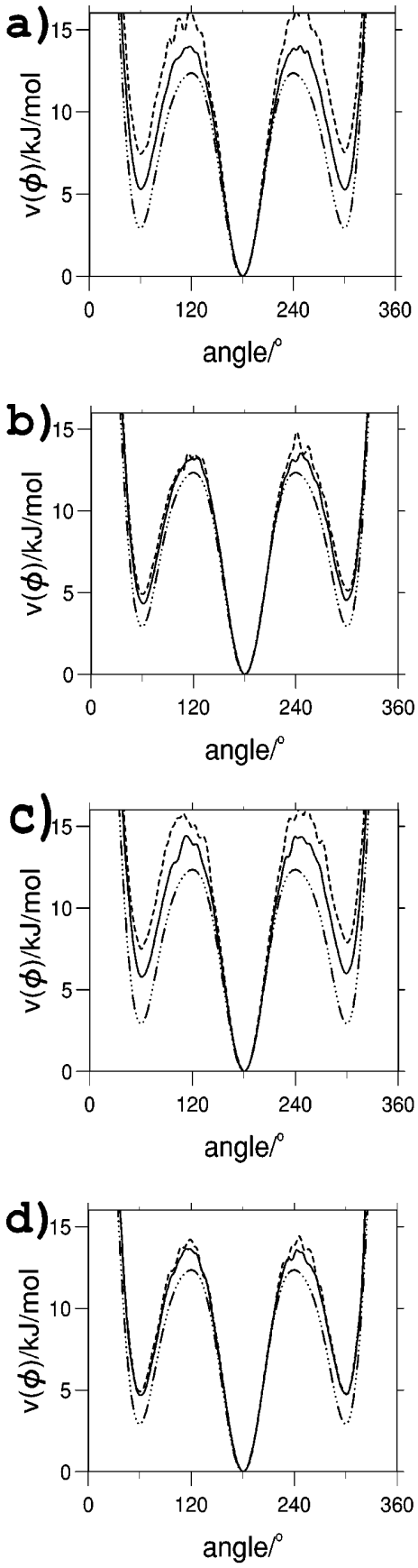

FIG. 8. Effective torsional potentials in NPT ensemble. (a) ϕ_1; (b) ϕ_2; (c) ϕ_3; (d) ϕ_4: bold line—330 K (isotropic phase), dashed line—300 K (smectic-A phase), dot/dashed line—Ryckaert–Bellemans potential.

TABLE V. Most populated conformers for the flexible alkyl chain in NPT simulations for the smectic-A and isotropic liquid phases. t represents a *trans* conformer, g_+ and g_- represents *gauche* conformers. For g_+/g_- equivalent conformers (e.g., tg_+ttttt/tg_-ttttt), the mean population for the 2 conformers is quoted (errors $\pm 0.3\%$).

Conformer	% at 300 K	% at 330 K
$tttttt$	47.2	19.0
tg_+ttttt/tg_-ttttt	3.3	2.7
$ttttg_+t/ttttg_-t$	2.8	2.8
$tttg_+ttt/tttg_-ttt$	2.9	2.6
tg_+tg_-ttt/tg_-tg_+ttt	1.7	1.1
$tttg_+tg_-t/tttg_-tg_+t$	1.6	1.0
ttg_+ttt/ttg_-ttt	0.8	2.6
$tttttg_+/tttttg_-$	0.8	1.4
$tttg_+tt/tttg_-tt$	0.7	1.7
g_+ttttt/g_+ttttt	0.5	1.5

has the effect of increasing the energy difference between *gauche* and trans conformers ΔE_{gt} and raising barrier heights for conformer interconversion. Both these factors show a strong odd–even effect with the odd dihedrals effected most strongly. The reason for this can be seen in Table V where the populations of the most favoured of the 3^7 possible chain conformers are listed for the isotropic and smectic-A phases. The influence of smectic order is to strongly promote those conformations in which the molecule remains linear. In Table V the *all-trans* conformation (*tttttt*) is strongly favoured by a change to a smectic-A phase, and *gauche* conformations *tgttttt*, *tttgttt*, *tttttgt* in which the molecule remains more linear are selected in favor of *gauche* conformations *gttttt*, *ttgtttt*, *tttgttt*, *ttttgtt*, *tttttg* in which the *gauche* linkage causes a major departure from molecular linearity. The latter are less abundant in the smectic-A phase than four conformers containing two *gauche* bonds (e.g., tg_+tg_-ttt). In the case of these conformers the energy gained in keeping the molecule linear is sufficient to overcome the intramolecular energy penalty of having two *gauche* linkages. These results are consistent with those of molecular field theory. For 4-n-alkyl-4'-cyanobiphenyl mesogens 5CB (C_5 chain) and 8CB (C_8 chain) molecular field theory also predicts an enhancement in populations for linear conformers[46,47] with increasing order parameter, and these results have been used to successfully interpret quadrupolar couplings from NMR studies of the deuterated compounds.[48]

A number of other workers have examined conformational distributions for mesogens in a nematic phase, and it is of some interest to compare their results with those obtained for smectic phases in this study. Wilson and Allen[21] have considered the mesogen *trans*-4-(*trans*-4-n-pentylcyclohexyl)cyclohexylcarbonitrile (CCH5) and report runs in excess of 700 ps in the nematic phase. They report an increase in the energy gap between *gauche* and *trans* conformers ΔE_{gt} from a pretransitional NPT simulation at 390 K to a nematic simulation at 350 K with an order parameter of 0.62. Starting from the end of the alkyl chain the increase in ΔE_{gt} values for CCH5 dihedrals are respectively 1.1, 0.03, 0.72 kJ/mol. These results are comparable with those obtained in this work (quoted in Table VI). The slightly

Downloaded 28 Sep 2005 to 129.234.4.10. Redistribution subject to AIP license or copyright, see http://jcp.aip.org/jcp/copyright.jsp

TABLE VI. Differences in energy ΔE_{gt} between *gauche* and *trans* conformers in units of kJ mol^{-1}. (Errors ± 0.3 kJ mol^{-1}.)

Dihedral	ΔE_{gt}(300 K) (isotropic)	ΔE_{gt}(330 K) (smectic-A)	ΔE_{gt}(330 K) $-\Delta E_{gt}$(300 K)
ϕ_1	5.4	7.5	2.1
ϕ_2	4.5	5.0	0.5
ϕ_3	5.9	7.7	1.8
ϕ_4	4.7	4.9	0.2
ϕ_5	6.0	8.0	2.0
ϕ_6	4.5	5.3	0.8
ϕ_7	5.2	7.5	2.3

larger values in Table VI being directly attributable to the slightly larger change in both S_2 and system density for the isotropic liquid to smectic-A phase change. Cross and Fung[28] also report an odd–even effect for chain dihedrals seen in atomistic simulations of 80 5CB molecules. As in this work, Cross and Fung have attributed this effect to the coupling between molecular conformation and the orientational mean field arising from neighbouring molecules in the fluid.

IV. CONCLUSIONS

A general model has been described which allows the simulation of anisotropic molecules made from a combination of Lennard-Jones sites and Gay-Berne potentials. The model has been used to study the phase behavior of a liquid crystal dimer molecule composed of two Gay-Berne potentials linked by a semi-flexible alkyl chain. The model simulated exhibits isotropic liquid, smectic-A and smectic-B phases, identified through examination of S_2, $g_\parallel$, $g_\perp$, g_2 for Gay-Berne units and through visualization of configuration snapshots. In both NVT and NPT studies the simulations time required to grow a smectic-A phase from an isotropic liquid is approximately 6 ns. Molecules remain flexible in the smectic-A phase and freely undergo conformational changes to and from *gauche*/*trans* conformers. A strong odd–even effect is exhibited in bond order parameters in the alkyl chains, and a strong coupling between molecular environment and molecular conformation is seen. The latter leads to an enhancement in the populations of linear conformers, and effective torsional angle potentials which are strongly influenced by molecular environment.

The simulation methods employed in this study have many potential applications. The use of Gay-Berne potentials to replace rigid parts of the molecule provides substantial savings in computer time over fully atomistic models. This opens the way for the simulation of polymer liquid crystal materials, for both main-chain and side-chain systems. There is however considerable work required before models of this type may be used to quantitatively predict phase behavior of real systems. For example, the phase behavior of real α, ω-bis(4,4'-cyanobiphenyloxy)alkyl homologues[32] are rather different to the Gay-Berne dimer system studied here. In the real homologues only nematic mesophases have been observed. This would suggest that segregation into aromatic-rich and aliphatic-rich sub-layers is not strongly favoured for these systems. In the present work the preference for microphase separation into Gay-Berne rich and Lennard-Jones domains is visible in the pretransitional region of the isotropic phase and at lower temperatures this leads to the formation of smectic phases. It would be possible to vary the relative strengths given to Gay-Berne/Gay-Berne and Gay-Berne/Lennard-Jones interactions, increasing the latter is likely to destabilize smectic-A and smectic-B phases in favor of nematics. However, at the present time, no systematic parameterisation of Gay-Berne/atom interactions exists. Considerable work is still required in this area before models of the type described in this study can be used in the prediction of transition temperatures and phases for real mesogenic molecules.

ACKNOWLEDGMENTS

The author would like to thank the University of Durham for providing computer time on its parallel SGI R10000 machine and providing a grant towards the purchase of a R10000 workstation; and the UK EPSRC for providing computer time on the Cray T3D in Edinburgh. The author gratefully acknowledges valuable discussions with Alexey V. Lyulin and Michael P. Allen (University of Bristol) and thanks them for their encouragement in developing the generalized parallel simulation code GBMOL.

[1] M. P. Allen and M. R. Wilson, J. Comput. Aided Mol. Design, **3**, 335 (1989).
[2] D. Frenkel, B. M. Mulder, and J. P. McTague, Phys. Rev. Lett. **52**, 287 (1984).
[3] D. Frenkel and B. M. Mulder, Mol. Phys. **55**, 1171 (1985).
[4] D. Frenkel and R. Eppenga, Phys. Rev. Lett. **49**, 1089 (1982).
[5] P. J. Camp and M. P. Allen, J. Chem. Phys. **106**, 6681 (1997).
[6] M. P. Allen, Liq. Cryst. **8**, 499 (1990).
[7] D. Frenkel, J. Phys. Chem. **92**, 3280 (1988).
[8] S. C. McGrother, D. C. Williamson, and G. Jackson, J. Chem. Phys. **104**, 6755 (1996).
[9] T. Kihara Adv. Chem. Phys. **5**, 147 (1963).
[10] B. J. Berne and P. Pechukas, J. Chem. Phys. **56**, 4213 (1972).
[11] J. G. Gay and B. J. Berne, J. Chem. Phys. **74**, 3316 (1981).
[12] E. de Miguel, L. F. Rull, M. K. Chalam, and K. E. Gubbins, Mol. Phys. **74**, 405, (1991).
[13] G. R. Luckhurst, R. A. Stephens, and R. W. Phippen, Liq. Cryst. **8**, 451, (1990).
[14] G. R. Luckhurst and Simmonds, Mol. Phys. **80**, 233 (1993).
[15] M. A. Bates and G. R. Luckhurst, J. Chem. Phys. **104**, 6696 (1996).
[16] M. P. Allen, M. A. Warren, M. R. Wilson, A. Sauron, and W. Smith, J. Chem. Phys. **105**, 2850 (1996).
[17] E. de Miguel, E. M. del Rio, J. T. Brown, and M. P. Allen, J. Chem. Phys. **105**, 4234 (1996).
[18] J. T. Brown, Ph. D. thesis, University of Bristol, Chap. 3, (1997).
[19] D. J. Cleaver, C. M. Care, M. P. Allen, and M. P. Neal, Phys. Rev. E. **53**, 1 (1996).
[20] M. R. Wilson and M. P. Allen, Mol. Cryst. Liq. Cryst. **198**, 465 (1991).
[21] M. R. Wilson and M. P. Allen, Liq. Cryst. **12**, 157 (1992).
[22] S. J. Picken, W. F. van Gunsteren, P. Th. van Duijnen, and W. H. de Jeu, Liq. Cryst. **6**, 357 (1989).
[23] B. Jung and B. L. Schürmann, Mol. Cryst. Liq. Cryst. **185**, 141 (1990).
[24] A. V. Komolkin, Yu. V. Molchanov, and P. P. Yakutseni, Liq. Cryst. **6**, 39, (1989).
[25] I. Ono and S. Kondo, Mol. Cryst. Liq. Cryst. **8**, 69, (1991).
[26] I. Ono and S. Kondo, Bull. Chem. Soc. Jpn. **65**, 1057, (1992).
[27] I. Ono and S. Kondo, Bull. Chem. Soc. Jpn. **66**, 633, (1993).
[28] C. W. Cross and B. M. Fung, J. Chem. Phys. **101**, 6839 (1994).

Downloaded 28 Sep 2005 to 129.234.4.10. Redistribution subject to AIP license or copyright, see http://jcp.aip.org/jcp/copyright.jsp

[29] J. Huth, T. Mosell, K. Nicklas, A. Sariban, and J. Brickmann, J. Phys. Chem. **98**, 7685, (1994).
[30] M. Yoneya and H. J. C. Berendsen, J. Phys. Soc. Jpn. **63**, 1025 (1994).
[31] G. Krömer, D. Paschek, and A. Geiger, Ber. Bunsenges. Phys. Chem. **97**, 1188 (1993).
[32] J. W. Emsley, G. R. Luckhurst, and G. N. Shilstone, Mol. Cryst. Liq. Cryst. **102**, 223 (1984).
[33] J. W. Emsley, G. R. Luckhurst, and G. N. Shilstone, Mol. Phys. **53**, 1023 (1984).
[34] D. A. Dunmur and M. R. Wilson, J. Chem. Soc. Faraday Trans. 2 **84**, 1109 (1988).
[35] G. La Penna, D. Catalano, and C. A. Veracini, J. Chem. Phys. **105**, 7097 (1996).
[36] J. P. Ryckaert and A. Bellemans, Chem. Phys. Lett. **30**, 123 (1990).
[37] S. Leggetter and D. J. Tildesley, Mol. Phys. **68**, 519 (1989).
[38] J. Alejandre, J. W. Emsley, D. J. Tildesley, and P. Carlson, J. Chem. Phys. **101**, 7027 (1994).
[39] D. Fincham, CCP5 Q. **12**, 47 (1984).
[40] M. R. Wilson, M. P. Allen, M. A. Warren, A. Sauron, and W. Smith, J. Comput. Chem. **18**, 478 (1997).
[41] J. P. Ryckaert, Mol. Phys. **55**, 549, (1985).
[42] T. A. Andrea, J. Chem. Phys. **79**, 4576 (1983).
[43] H. C. Anderson, J. Chem. Phys. **72**, 2384 (1980).
[44] R. Eppenga and D. Frenkel, Mol. Phys. **52**, 1303 (1984).
[45] M. R. Wilson and M. P. Allen, Mol. Phys. **80**, 277 (1993).
[46] J. W. Emsley, G. R. Luckhurst, and C. P. Stockley, Proc. R. Soc. London, Ser. A, **381**, 139 (1982).
[47] M. R. Wilson, Liq. Cryst. **21**, 437 (1996).
[48] J. W. Emsley, G. R. Luckhurst, and C. P. Stockley, Mol. Phys. **44**, 565 (1981).

Downloaded 28 Sep 2005 to 129.234.4.10. Redistribution subject to AIP license or copyright, see http://jcp.aip.org/jcp/copyright.jsp